Research Article Vol. 40, No. 11 / November 2023 / Journal of the Optical Society of America B 2913

Journal of the Optical Society of America B OPTICAL PHYSICS

Design of a multi-core photonic crystal fiber supporting 518 OAM modes

Qiang Liu,[1,2] Mingzhu Han,[1,2] Haiwei Mu,[1,2] Wei Liu,[1,2] Wenjing Li,[1,2] Kaiyu Wang,[1,2] Chao Ma,[1,2] Jingwei Lv,[1,2] Paul K. Chu,[3] and Chao Liu[1,2,*]

[1]School of Physics and Electronic Engineering, Northeast Petroleum University, Daqing 163318, China
[2]SANYA Offshore Oil & Gas Research Institute, Northeast Petroleum University, Sanya 572024, China
[3]Department of Physics, Department of Materials Science & Engineering, and Department of Biomedical Engineering, City University of Hong Kong, Tat Chee Avenue, Kowloon, Hong Kong, China
*msm-liu@126.com

Received 24 July 2023; revised 19 September 2023; accepted 2 October 2023; posted 3 October 2023; published 24 October 2023

A multi-ring core photonic crystal fiber (PCF) with seven high-index ring regions is designed for the transmission of multiple orbital angular momentum (OAM) modes. The new structure which has an optimized air hole arrangement shows improved transmission quantity and number of OAM modes. Numerical analysis reveals that the PCF can transmit 518 OAM modes in the range of 1.4–1.75 μm stably while avoiding cross talk from the adjacent ring core resulting in a low cross talk of merely −208.5 dB, confinement loss less than 10^{-9} dB/m, as well as mode quality greater than 0.925. The results disclose a new method to increase the communication capacity and suggest that the PCF has great application potential.

https://doi.org/10.1364/JOSAB.501502

1. INTRODUCTION

With the rapid development of information technology, the large amount of data required by big data, cloud computing, and other application requires a higher optical fiber communication capacity. The space-division multiplexing technology is an effective method to enhance the transmission capacity of optical fibers [1–3] and consequently, multi-core fiber and mode-division multiplexing technologies have become research hotspots. The multi-core fiber refers to adding a multiple fiber core to a single fiber to achieve space-division multiplexing, while mode-division multiplexing can be attained by few-mode optical fibers. Recently, orbital angular momentum (OAM) multiplexing techniques have provided a new solution to expand the communication capacity. OAM is characterized by a helical phase front that twists around the axis of propagation [4–6]. Owing to the discrete helical phase, the OAM eigenstates are infinite and orthogonal to each other, so that each OAM mode can be used as an independent channel to improve the transmission capacity and realize infinite orthogonal channels theoretically. However, OAM beams are formed by linear superposition of four vector eigenmodes of the same order and therefore, the effective refractive index difference between the eigenmodes is required to be greater than 1×10^{-4}, otherwise it will degenerate into linear polarization modes during transmission. Hence, the traditional single-mode fiber cannot support the stable transmission of OAM modes [7–9]. In order to accomplish simultaneous transmission of multiple OAM modes, it is necessary to design a fiber to meet the transmission requirements. At present, the vortex fiber [10], ring core fiber [11], and ring-like core fiber [12] have been demonstrated to transmit OAM modes, but the supported OAM mode number is limited due to the restriction of the fiber structure.

Recently, the photonic crystal fiber (PCF) has been adopted to design OAM mode transmission fibers. PCF boasts advantages such as the flexible structure design, low transmission loss, and controllable nonlinearity [13,14] and can achieve low-loss transmission of multiple OAM modes with high mode quality. For example, Yue *et al.* have designed a PCF structure composed of As_2S_3 that can transmit two OAM modes simultaneously [15] and Tian *et al.* have proposed an orbital angular momentum photonic crystal fiber made of silica consisting of a large air hole in the center and four layers air holes in the cladding area. By optimizing the arrangement of air holes, the number of OAM modes can be increased [16]. Bai *et al.* have proposed a PCF with square pores that can support 58 OAM modes with a confinement loss (CL) of less than 10^{-9} dB/m [17], and Lei *et al.* have designed a semi-circular air hole PCF that can transmit 66 OAM modes with a confinement loss of less than 10^{-9} dB/m and nonlinear coefficient of less than $4\ W^{-1}\ km^{-1}$ [18]. Zhang *et al.* have used a high refractive index ring core to achieve 110 OAM modes transmission and observed that the number of transmitted OAM modes can be increased by increasing the refractive index difference between the layered core and cladding [19]. Phosphate glass, SF_2, SSK_2, GeO_2, Schott SF_6, and other high

refractive index materials have been used as the ring core materials [20–23]. It has been shown that the effective method to increase the number of OAM modes is to increase the effective refractive index difference between the eigenmodes. In order to achieve the goal, the feasible way is to increase the filling ratio of the air holes by optimizing the air hole distribution or to directly use ring core materials with a high refractive index. In our previous research, we increased the number of OAM modes with a special PCF structure and demonstrated that multi-core fibers could support multiple OAM modes [24–30]. At the same time, Wang *et al.* [31] and Han *et al.* [32] have designed double-layer concentric ring core and three-layer concentric ring core PCF structures to further increase the number of OAM modes. Chen *et al.* have also proposed a 19 ring core optical fiber made of SiO_2 but because of the limitations of the conventional optical fiber structures, each ring core can only transmit 34 OAM modes at the wavelength of 60 nm.

Herein, a multi-core PCF consisting of seven ring cores is designed based on the three-layer hexagonal structure. The high refractive index ring core is introduced into the second layer and central air hole. The OAM transmission characteristics are studied by the full vector finite element method. The results show that the PCF can transmit 518 OAM modes stably in the wavelength range of 1.4–1.75 μm with low confinement loss, large mode field area, and low cross talk of adjacent cores of −202.5 dB. The structure has large potential in high-capacity optical fiber communication.

2. THEORY

The OAM modes are the linear superposition of the odd mode and even mode of the same order vector modes, HE mode and EH mode, in the fiber. When the effective refractive index difference between the vector modes is greater than 10^{-4}, the same order vector modes can form the OAM mode. The relationship is as follows [33]:

$$\mathrm{OAM}^{\pm}_{\pm l,m} = \mathrm{HE}^{\mathrm{even}}_{l+1,m} \pm j\mathrm{HE}^{\mathrm{odd}}_{l+1,m}, \tag{1}$$

$$\mathrm{OAM}^{\mp}_{\pm l,m} = \mathrm{EH}^{\mathrm{even}}_{l-1,m} \pm j\mathrm{EH}^{\mathrm{odd}}_{l-1,m}, \tag{2}$$

where l is the topological charge and m represents the radial mode order. The circular polarization of the OAM mode may be right or left, as indicated by the "±" superscript, and "*even*" and "*odd*" represent the even mode and odd mode of the corresponding eigenmode. The number of OAM modes supported by the optical fiber can be calculated by Eqs. (2) and (3). There are two OAM modes for $l = 1$ and four OAM modes for $l \geq 2$. Clearly, the transmission characteristics of the OAM modes depend on the corresponding eigenmodes.

The isolation parameter is an important factor for the multi-core fiber [34]. It is defined as the power cross talk of multi-core fiber and measures the fraction of the total energy leaking out into the ring core region. The isolation parameter is calculated as follows [35]:

$$\mathrm{ISO} = \frac{\iint_{\mathrm{ring}}(E_x H_y - E_y H_x)\mathrm{d}x\mathrm{d}y}{\iint_{\mathrm{total}}(E_x H_y - E_y H_x)\mathrm{d}x\mathrm{d}y}, \tag{3}$$

where E_x, E_y and H_x, H_y are the electric and magnetic field components of the corresponding modes.

The mode purity (η) plays an important role in OAM mode transmission and demultiplexing. A higher mode purity ensures stable transmission of OAM modes in the optical fiber as expressed below [36,37]:

$$\eta = \frac{I_r}{I_c} = \frac{\iint_{\mathrm{ring}} |\vec{E}|\mathrm{d}x\mathrm{d}y}{\iint_{\mathrm{whole-section}} |\vec{E}|^2\mathrm{d}x\mathrm{d}y}, \tag{4}$$

where E is the electric field intensity, and I_r and I_c represent the average intensity of the ring core and the whole section of the structure, respectively.

The CL is another critical parameter that describes the loss of the optical field energy during transmission and determines the transmission distance. In the multi-core PCF, the CL is related to the structural parameters and can be calculated using the imaginary part of the effective refractive index as follows [38,39]:

$$\mathrm{CL} = \frac{2\pi}{\lambda}\frac{20}{\ln 10}\mathrm{Im}(n_{\mathrm{eff}}), \tag{5}$$

where $\mathrm{Im}(n_{\mathrm{eff}})$ represents the imaginary part of the effective refractive index and λ is the wavelength.

Nonlinear effects in optical fibers can cause additional loss in the transmitted signal thus affecting the quality of mode transmission. The nonlinear effects may result in cross talk and decrease the signal-to-noise ratio. The nonlinear effect of the optical fiber is usually evaluated using the nonlinear coefficient as shown in the following [40]:

$$\gamma = \frac{2\pi n_2}{\lambda A_{\mathrm{eff}}}, \tag{6}$$

where n_2 refers to the nonlinear refractive index of the high refractive index ring GeO_2 and has a value of 2.783×10^{-20} $\mathrm{m^2\,w^{-1}}$ [41]. A_{eff} is the effective mode area defined as follows [42]:

$$A_{\mathrm{eff}} = \frac{\left(\iint |E(x,y)|^2\mathrm{d}x\mathrm{d}y\right)^2}{\iint |E(x,y)|^4\mathrm{d}x\mathrm{d}y}, \tag{7}$$

where $E(x, y)$ is the electric field intensity distribution. The effective mode field area is inversely proportional to the nonlinear coefficient and therefore, a large mode field area suppresses the nonlinear effect of the fiber.

3. FIBER STRUCTURE AND OPTIMIZATION

The cross section of the multi-core PCF is depicted in Fig. 1. It has a hexagonal structure with three layers of air holes. The high refractive index ring core composed of GeO_2 is introduced into the second layer and central air holes to form a PCF with seven ring cores. The refractive index of the GeO_2 [Eq. (8)] and SiO_2 [Eq. (9)] can be derived from the Sellmeier equation, as follows [43,44]:

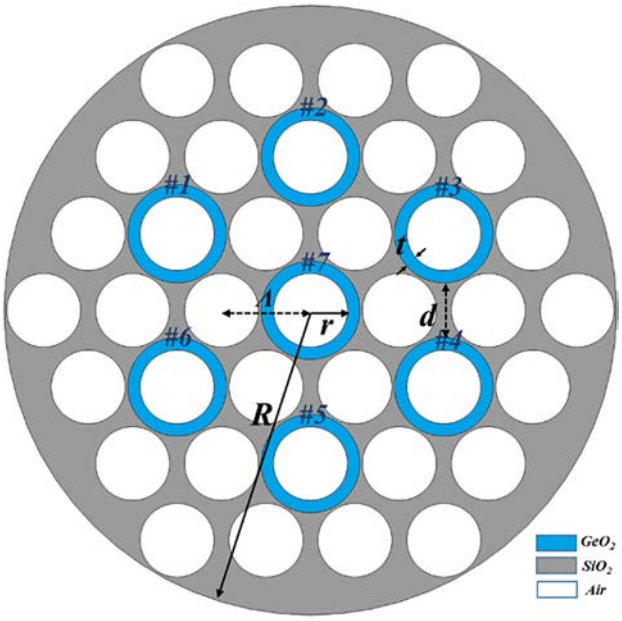

Fig. 1. Cross section of the designed seven-core PCF.

Table 1. Structural Parameters of the Multi-core PCF

Symbol	R	t	r	d	Λ
Value (μm)	62	2.5	7.5	$\sqrt{3}\Lambda - 2r - 2t$	$2.4\,r$

$$n^2(\lambda) = 1 + \frac{0.6961663\lambda^2}{\lambda^2 - 0.00467914826} + \frac{0.4079426\lambda^2}{\lambda^2 - 0.135120631} + \frac{0.8974794\lambda^2}{\lambda^2 - 97.9340025}. \tag{9}$$

The radius of the PCF and air holes are R and r, respectively. The thickness of the ring core is t, the spacing between adjacent air holes is Λ. The outer ring spacing of the adjacent ring core is d. The OAM modes can propagate simultaneously in the seven high refractive index ring cores with improved efficiency.

In order to maximize the number of supported OAM modes and minimum inter-core cross talk, the ring core thickness t, air hole radius r, and spacing Λ are optimized successively. The optimal parameters are listed in Table 1. Figure 2 shows the electric field diagrams of several typical modes in the #1 ring core, including $HE_{3,1}$, $EH_{1,1}$, $HE_{11,1}$, $EH_{9,1}$, $HE_{22,1}$, and $EH_{20,1}$. All the intrinsic modes are restricted in the ring core with good modal quality. On account of the symmetry of the PCF, the cross talk of #1 and #7 ring cores is analyzed as an example. Figure 3 shows the derived OAM mode number and inter-core cross talk XT_{mn} at 1.55 μm. The number of supported OAM modes increases with the ring core thickness and the maximum is obtained at $t = 2.5$ μm, as shown in Fig. 3(a). Each ring core can transmit 74 OAM modes and the total number of OAM modes is 518. However, the inter-core cross talk increases with the ring

$$n^2(\lambda) = 1 + \frac{0.80686642\lambda^2}{\lambda^2 - 0.068972606^2} + \frac{0.71815848\lambda^2}{\lambda^2 - 0.15396605^2} + \frac{0.85416831\lambda^2}{\lambda^2 - 11.84193^2}, \tag{8}$$

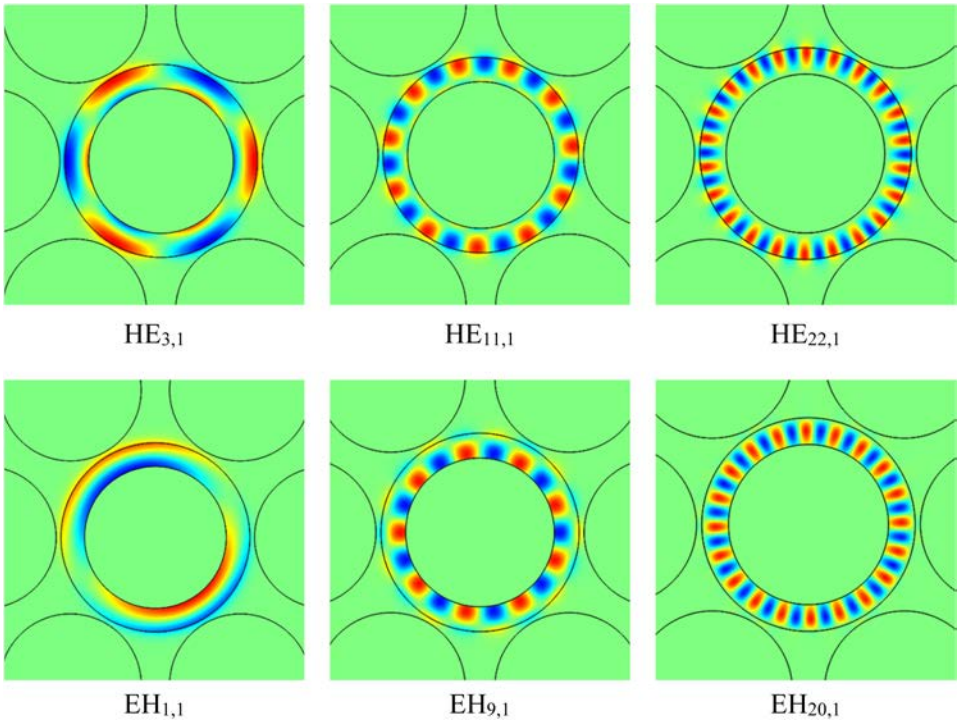

Fig. 2. Electric field intensity distributions of the typical vector eigenmodes in the #1 ring core.

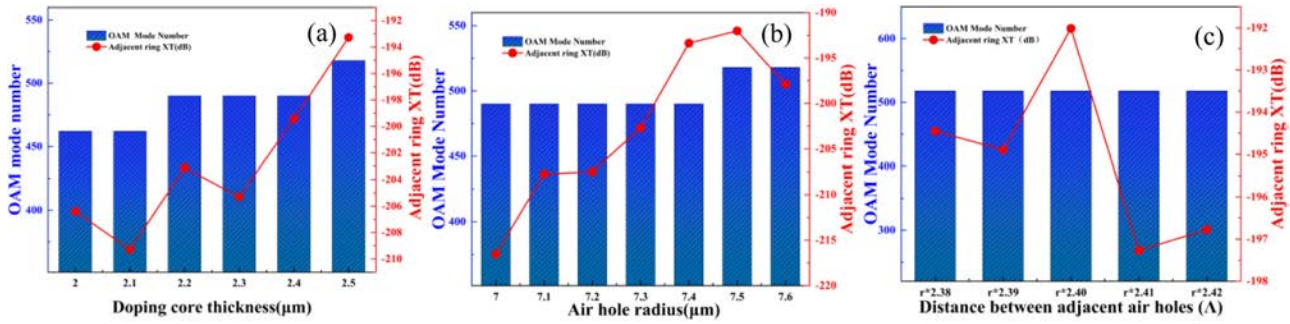

Fig. 3. Influence of different structural parameters on OAM transmission: (a) ring core thickness t, (b) air hole radius r, and (c) spacing Λ.

core thickness because increasing t will decrease the distance d of the adjacent rings. For t equal to 2.5 μm, the maximum cross talk is still low at −194 dB which can be ignored. Therefore $t = 2.5$ μm is chosen to be the optimal value. Similarly, the radius r of the air holes is optimized as shown in Fig. 3(b). For $r = 7.5$ μm and 7.6 μm the PCF supports the maximum OAM modes with lower cross talk. In order to control the distance of the air holes, $r = 7.5$ μm is determined as the optimal value. The distance Λ of the adjacent air holes is then optimized. As shown in Fig. 3(c), when Λ is changed from $r * 2.38$ to $r * 2.42$, it has little influence on the number of OAM modes and cross talk. It shows that the structure has good robustness and $\Lambda = r * 2.40$ is chosen as the optimal size.

4. RESULTS AND DISCUSSION

A. Effective Refractive Index and Refractive Index Difference

The effective refractive index of the HE mode and EH mode is shown in Figs. 4(a) and 4(b). In the wavelength range of 1.4–1.75 μm the effective refractive index decreases with increasing wavelength. The variation of the lower-order mode is relatively

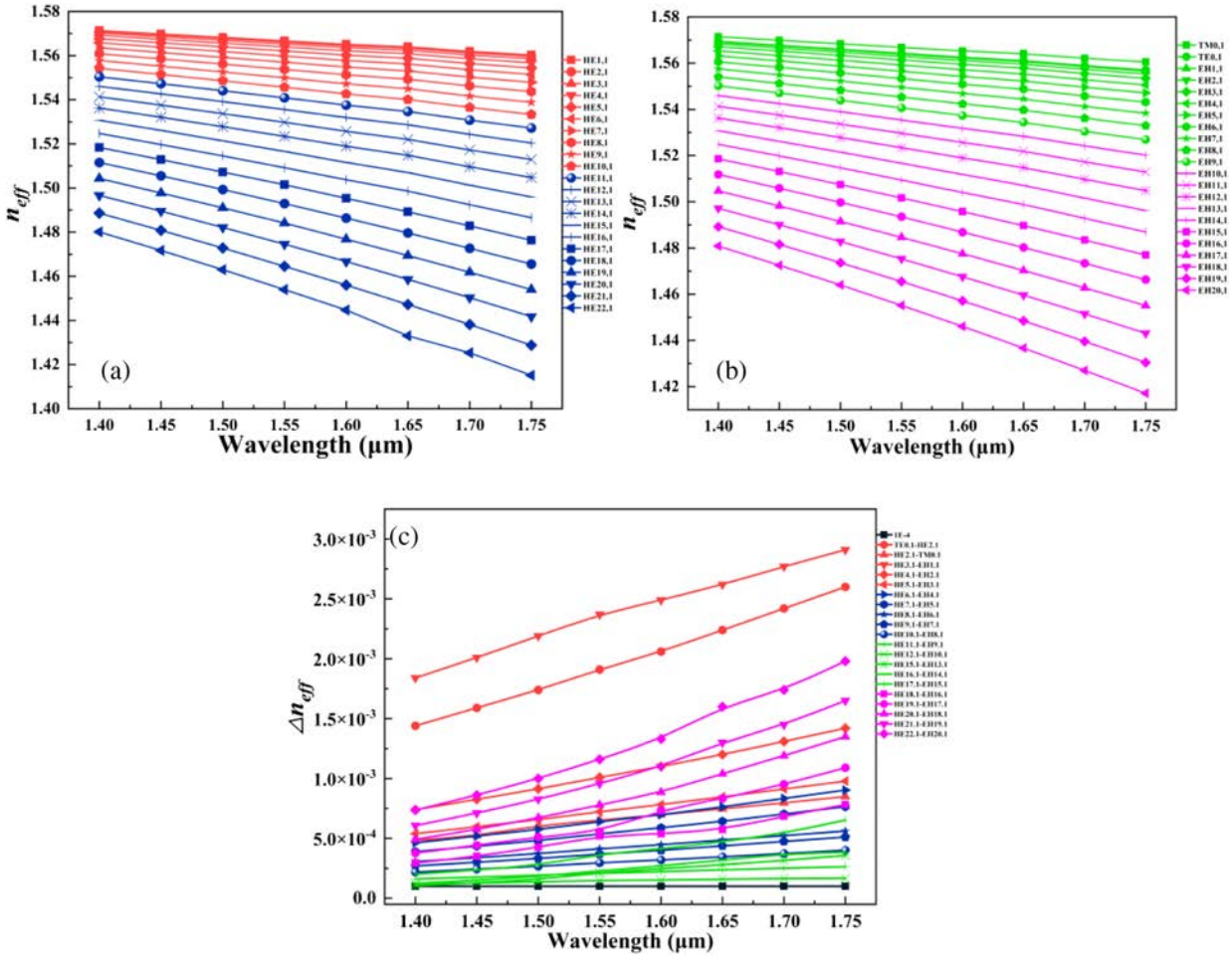

Fig. 4. Effective refractive indices of #1 ring core: (a) $HE_{l,1}$ modes, (b) $EH_{l,1}$ modes, and (c) effective refractive index difference.

flat and the effective refractive index of the higher-order mode is larger than that of lower-order modes.

The effective refractive index difference (Δ_{neff}) of the HE and EH modes constituting the OAM modes is shown in Fig. 4(c). All the effective refractive index differences are greater than 10^{-4} in the range of 1.4–1.75 μm and increase gradually with increasing wavelength. At 1.55 μm, the effective refractive index difference of the $HE_{3,1}$ mode and $EH_{1,1}$ mode is 2.9×10^{-3}. A larger effective refractive index difference can prevent the EH and HE modes from degenerating into the linear polarization mode to ensure the transmission quality.

B. Isolation Parameter

The isolation parameters of the typical eigenmodes of the #1 ring cores are calculated by Eq. (3) and the power cross talk values of the $HE_{1,1}$, $EH_{1,1}$, $HE_{11,1}$, $EH_{9,1}$, $HE_{22,1}$, and $EH_{20,1}$ modes are presented in Fig. 5. The isolation parameter of the above eigenmodes increases with wavelength, and the power cross talk of lower-order modes is as high as 208.5 dB in the range of 1.4–1.75 μm. The power cross talk of the high-order mode is larger with a changing range such as the $EH_{20,1}$ mode of 55–141 dB. It is because high-order modes exhibit relatively larger propagation characteristics and stronger coupling to the waveguide core within optical fibers or waveguides, making them more challenging to separate and maintain isolation in multi-mode optical fibers or waveguides.

C. Mode Purity

The mode purity of the supported eigenmodes is calculated by Eq. (4) and the results are shown in Fig. 6. The mode purity decreases with wavelength because the longer wavelength mode can easily leak from the ring core to the cladding. Meanwhile, the mode purity of all the eigenmodes is greater than 92.5% in the range of 1.4–1.75 μm and mostly concentrated between 96% and 98% with the highest value of 98.34% for the $HE_{1,1}$ mode. A higher mode purity improves the transmission stability boding well for OAM mode encoding and multiplexing.

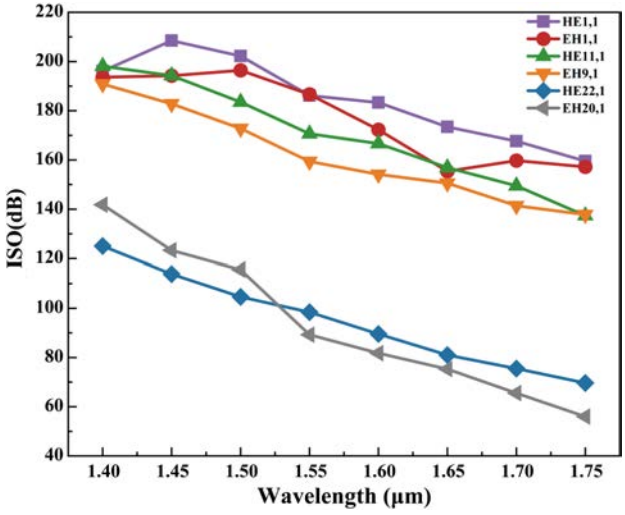

Fig. 5. Channel isolation of the typical modes.

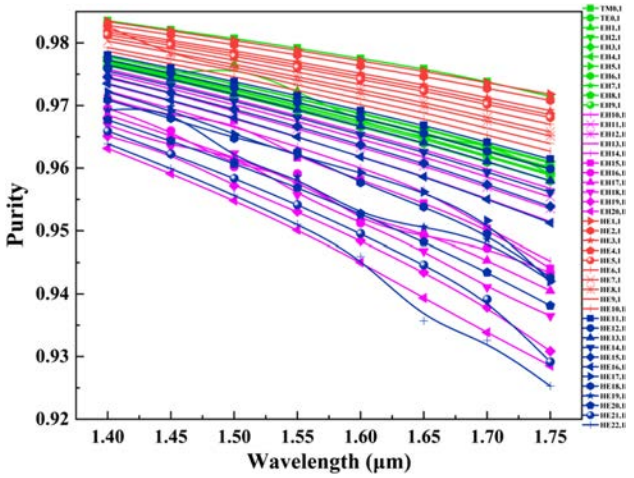

Fig. 6. Mode purity of the eigenmodes in the #1 ring core.

D. Confinement Loss

The confinement loss of the supported eigenmodes is calculated by Eq. (5) and the results are shown in Fig. 7. In the wavelength range of 1.4–1.75 μm, the confinement loss of the supported eigenmodes is as low as 10^{-12} dB/m − 10^{-9} dB/m, which is better than previous results [31,32] and also meets the requirement for long-distance transmission of OAM modes.

E. Nonlinear Coefficient and Effective Mode Field Area

The effective mode field area of the eigenmode is calculated by Eq. (7). In the wavelength range of 1.4–1.75 μm the effective mode field area of most eigenmodes is 100−118 μm^2, as shown in Fig. 8(a). At 1.55 μm, the maximum effective mode field area is 118.68 μm^2. A larger mode field area reduces the nonlinear effect and improves the signal-to-noise ratio of the system. The nonlinear coefficient of the transmission eigenmode is calculated by Eq. (6) as shown in Fig. 8(b). Obviously, the nonlinear coefficient decreases with increasing wavelength. The nonlinear coefficients of all the eigenmodes of the multi-core PCF are less than 1.20 $W^{-1} \cdot km^{-1}$. In particular, the nonlinear coefficient

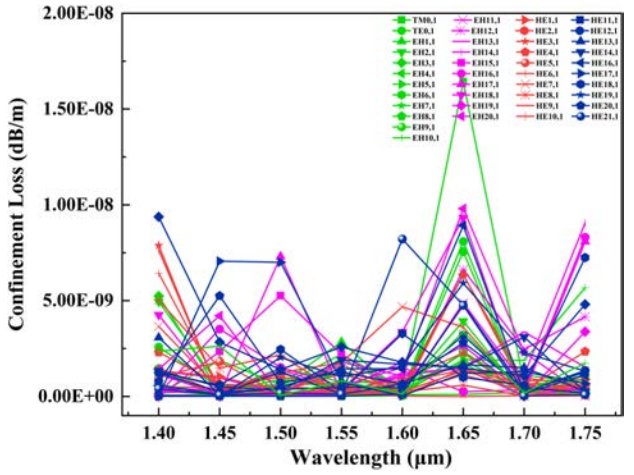

Fig. 7. Confinement loss of the supported eigenmodes in the #1 ring core fiber.

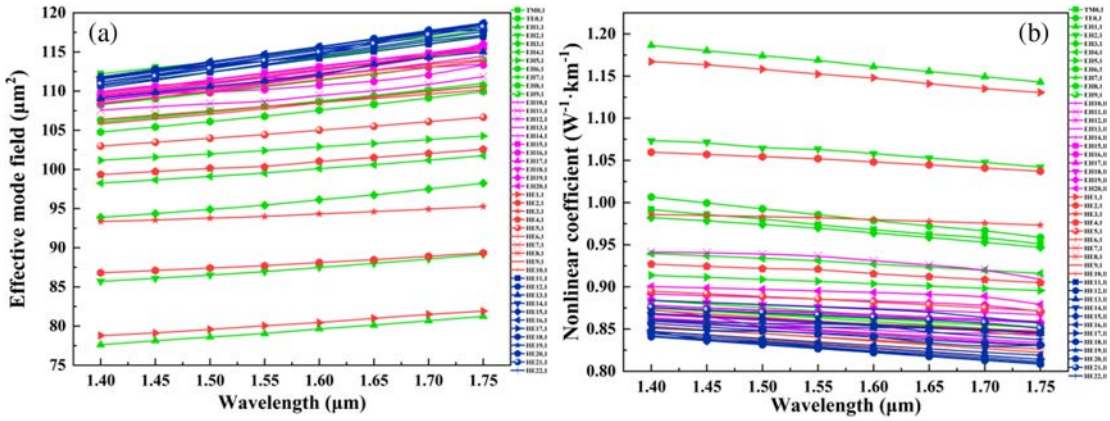

Fig. 8. (a) Effective mode field area and (b) nonlinear coefficients of the eigenmodes in the #1 ring core.

Table 2. Comparison of the Properties of the Proposed PCF and Previously Reported PCFs

References	Operating Band (nm)	Supported OAM Modes	OAM Purity	Confinement Loss dB · m^{-1}	Nonlinearity Coefficient W^{-1} km^{-1}
[23]	1400–1700	$56+4lp$	0.8	4.91×10^{-8}	—
[31]	1520–1580	$30+50$	—	$<10^{-8}$	<2.65
[32]	1500–2000	$46+62+74$	0.91–0.98	$10^{-12}-10^{-8}$	0.22–1.04
	1520–1580	36×19	—	—	—
This work	1400–1750	74×7	0.92–0.98	$10^{-12}-10^{-9}$	0.82–1.2

of the $TM_{0,1}$ mode is only 0.82 $W^{-1}\cdot km^{-1}$ at 1.55 μm and those of the higher-order modes are less than those of the lower-order modes. The nonlinear coefficient of most eigenmodes is less than 1.05 $W^{-1}\cdot km^{-1}$ at 1.55 μm indicating excellent performance.

Finally, the comparison of the properties of the proposed structure and those reported multi-core PCFs recently is shown in Table 2. The proposed ring core PCF can transmit more OAM modes in single ring core and can support 518 OAM modes transmission with lower confinement loss and high purity in a wider wavelength range. The comprehensive performance is superior to the previously reported PCFs.

5. CONCLUSION

A new large-capacity multi-core PCF is designed for transmission of multiple OAM modes and analyzed by the finite element method. The PCF supports the transmission of 518 OAM modes in the wavelength range of 1.4–1.75 μm. Meanwhile, the supported eigenmodes exhibit high mode purity and low nonlinear coefficients as exemplified by low confinement losses of $10^{-12}-10^{-9}$ dB/m. The multi-core PCF has great potential in optical fiber communication.

Funding. Provincial Talent Project (ts26180221); Hainan Province Science and Technology Special Fund (ZDYF2022GXJS003); Local Universities Reformation and Development Personnel Training Supporting Project from Central Authorities; Natural Science Foundation of Heilongjiang Province (grant number LH2021F007); China Postdoctoral Science Foundation funded project (grant number 2020M670881); City University of Hong Kong Strategic Research Grant (SRG) (grant number 7005505); City University of Hong Kong Donation Research Grant (grant number DON-RMG 9229021).

Acknowledgment. This work was jointly supported by the Provincial Talent Project, Hainan Province Science and Technology Special Fund, Local Universities Reformation and Development Personnel Training Supporting Project from Central Authorities, Natural Science Foundation of Heilongjiang Province, China Postdoctoral Science Foundation funded project, City University of Hong Kong Strategic Research Grant (SRG), and City University of Hong Kong Donation Research Grant.

Disclosures. The authors declare no conflicts of interest.

Data availability. Data underlying the results presented in this paper are not publicly available at this time but may be obtained from the authors upon reasonable request.

REFERENCES

1. R. Ryf, S. Ryf, A. H. Gnauck, C. Bolle, A. Sierra, S. Mumtaz, M. Esmaeelpour, E. C. Burrows, R. J. Essiambre, P. J. Winzer, and D. W. Peckham, "Mode-division multiplexing over 96 km of few-mode fiber using coherent 6×6 MIMO processing," J. Lightwave Technol. **30**, 521–531 (2012).
2. S. Randel, R. Ryf, A. Sierra, P. J. Winzer, A. H. Gnauck, C. A. Bolle, R. J. Essiambre, D. W. Peckham, A. McCurdy, and R. Lingle, "6× 56-Gb/s mode-division multiplexed transmission over 33-km few-mode fiber enabled by 6× 6 MIMO equalization," Opt. Express **19**, 16697–16707 (2011).
3. N. Bozinovic, Y. Yue, Y. Ren, M. Tur, P. Kristensen, H. Huang, A. E. Willner, and S. Ramachandran, "Terabit-scale orbital angular momentum mode division multiplexing in fibers," Science **340**, 1545–1548 (2013).
4. A. M. Yao and M. J. Padgett, "Orbital angular momentum: origins, behavior and applications," Adv. Opt. Photonics **3**, 161–204 (2011).
5. S. Ramachandran, P. Kristensen, and M. F. Yan, "Generation and propagation of radially polarized beams in optical fibers," Opt. Lett. **34**, 2525–2527 (2009).
6. A. E. Willner, H. Huang, Y. Yan, Y. Ren, N. Ahmed, G. Xie, C. Bao, L. Li, Y. Cao, Z. Zhao, and J. Wang, "Optical communications using orbital angular momentum beams," Adv. Opt. Photonics **7**, 66–106 (2015).
7. L. Schares, B. G. Lee, F. Checconi, R. Budd, A. Rylyakov, N. Dupuis, F. Petrini, C. L. Schow, P. Fuentes, O. Mattes, and C. Minkenberg, "A

throughput-optimized optical network for data-intensive computing," IEEE Micro **34**, 52–63 (2014).
8. R. J. Essiambre, G. J. Foschini, G. Kramer, and P. J. Winzer, "Capacity limits of information transport in fiber-optic networks," Phys. Rev. Lett. **101**, 163901 (2008).
9. C. Chen, G. Zhou, G. Zhou, M. Xu, Z. Hou, C. Xia, and J. Yuan, "A multi-orbital-angular-momentum multi-ring micro-structured fiber with ultra-high-density and low-level crosstalk," Opt. Commun. **368**, 27–33 (2016).
10. E. G. Johnson, J. Stack, and C. Koehler, "Light coupling by a vortex lens into graded index fiber," J. Lightwave Technol. **19**, 753–758 (2001).
11. G. Zhou, C. Chen, M. Xu, C. Xia, and Z. Hou, "Design and analysis of a microstructure ring fiber for orbital angular momentum transmission," IEEE Photonics J. **8**, 7802512 (2016).
12. N. Xia and S. Yoo, "Suppression of transverse mode instability in ring-core fiber," in *Conference on Lasers and Electro-Optics (CLEO)* (2020), pp. 1–2.
13. W. Liu, Y. Shi, Z. Yi, C. Liu, F. Wang, X. Li, J. Lv, L. Yang, and P. K. Chu, "Surface plasmon resonance chemical sensor composed of a microstructured optical fiber for the detection of an ultra-wide refractive index range and gas-liquid pollutants," Opt. Express **29**, 40734–40747 (2021).
14. C. Liu, J. Liu, W. Liu, F. Wang, and P. K. Chu, "Overview of refractive index sensors comprising photonic crystal fibers based on the surface plasmon resonance effect," Chin. Opt. Lett. **19**, 102202 (2021).
15. Y. Yue, L. Zhang, Y. Yan, N. Ahmed, J. Y. Yang, H. Huang, Y. Ren, S. Dolinar, M. Tur, and A. E. Willner, "Octave-spanning supercontinuum generation of vortices in an As_2S_3 ring photonic crystal fiber," Opt. Lett. **37**, 1889–1891 (2012).
16. W. Tian, H. Zhang, X. Zhang, L. Xi, W. Zhang, and X. Tang, "A circular photonic crystal fiber supporting 26 OAM modes," Opt. Fiber Technol. **30**, 184–189 (2016).
17. X. Bai, H. Chen, Y. Ma, and H. Yang, "Circular-lattice photonic crystal fiber with square air holes supporting 58 OAM modes," in *Progress In Electromagnetics Research Symposium-Spring (PIERS)* (2017), pp. 3105–3108.
18. Y. Lei, X. Xu, N. Wang, and H. Jia, "Numerical analysis of a photonic crystal fiber for supporting 76 orbital angular momentum modes," J. Opt. **20**, 105701 (2018).
19. L. Zhang, K. Zhang, J. Peng, J. Deng, Y. Yang, and J. Ma, "Circular photonic crystal fiber supporting 110 OAM modes," Opt. Commun. **429**, 189–193 (2018).
20. J. B. Lee, H. J. Choi, S. Y. Yoon, B. K. Kim, and H.-C. Park, "Processing of porous hydroxyapatite scaffolds containing calcium phosphate glass-ceramics for bone tissue engineering," J. Ceram. Process. Res. **14**, 544–548 (2013).
21. F. A. Al-Zahrani and K. Al-Zahrani, "Novel design of dual guided photonic crystal fiber for large capacity transmission in high-speed optics communications with supporting good quality OAM and LP modes," Alexandria Eng. J. **59**, 4889–4899 (2020).
22. W. Geng, Y. Fang, Y. Wang, Y. Li, C. Bao, H. Zhang, H. Huang, Y. Ren, Z. Pan, and Y. Yue, "Highly dispersive Ge-doped coupled ring fiber for high-order OAM modes," Proc. SPIE **11547**, 1154716 (2020).
23. W. Wang, N. Wang, K. Li, Z. Geng, and H. Jia, "A novel dual guided modes regions photonic crystal fiber with low crosstalk supporting 56 OAM modes and 4 LP modes," Opt. Fiber Technol. **57**, 102213 (2020).
24. Q. Liu, W. Lu, Y. Sun, J. Lv, W. Liu, C. Liu, S. Tai, B. Li, J. Zhao, Y. Jiang, and T. Sun, "A novel photonic quasi-crystal fiber for transmission of orbital angular momentum modes," Optik **251**, 168446 (2022).
25. Q. Liu, S. Tai, W. Lu, J. Sun, T. Lv, C. Liu, Y. Sun, J. Lv, W. Liu, T. Sun, and P. K. Chu, "Design of pure silica-based photonic crystal fiber for supporting 114 OAM modes transmission," J. Opt. **23**, 095701 (2021).
26. Q. Liu, S. Tai, Y. Sun, W. Lu, M. Han, J. Wang, C. Liu, J. Lv, W. Liu, and P. K. Chu, "A photonic quasi-crystal fibre supporting stable transmission of 150 OAM modes with high mode quality and flat dispersion," J. Mod. Opt. **69**, 887–896 (2022).
27. Q. Liu, S. Tai, Y. Sun, M. Han, J. Wang, C. Liu, J. Lv, S. Wang, G. Sun, and P. K. Chu, "Simple ring-structured photonic crystal fiber with low nonlinear coefficients and flat dispersion supporting 166 OAM modes," Opt. Eng. **61**, 076108 (2022).
28. H. Fu, C. Liu, Z. Yi, X. Song, X. Li, Y. Zeng, J. Wang, J. Lv, L. Yang, and P. K. Chu, "A new technique to optimize the properties of photonic crystal fibers supporting transmission of multiple orbital angular momentum modes," J. Opt. **52**, 307–316 (2023).
29. H. Fu, Y. Shi, Z. Yi, C. Liu, X. Song, J. Lv, L. Yang, and P. K. Chu, "Effects of air holes in the cladding of photonic crystal fibers on dispersion and confinement loss of orbital angular momentum modes," Opt. Quantum Electron. **54**, 353 (2022).
30. H. Fu, M. Zhu, C. Liu, Z. Yi, J. Lv, L. Yang, F. Wang, Q. Liu, W. Su, X. Li, and P. K. Chu, "Photonic crystal fiber supporting 394 orbital angular momentum modes with flat dispersion, low nonlinear coefficient, and high mode quality," Opt. Eng. **61**, 026111 (2022).
31. W. Wang, C. Sun, N. Wang, and H. Jia, "A design of nested photonic crystal fiber with low nonlinear and flat dispersion supporting 30+ 50 OAM modes," Opt. Commun. **471**, 125823 (2020).
32. M. Han, Q. Liu, Y. Sun, S. Tai, S. Wang, H. Fu, J. Wang, J. Lv, P. K. Chu, and C. Liu, "A novel nested three-ring-core photonic crystal fiber for OAM transmission," Optik **270**, 169981 (2022).
33. C. Brunet, P. Vaity, Y. Messaddeq, S. LaRochelle, and L. A. Rusch, "Design, fabrication and validation of an OAM fiber supporting 36 states," Opt. Express **22**, 26117–26127 (2014).
34. M. Zhu, W. Zhang, L. Xi, X. Tang, and X. Zhang, "A new designed dual-guided ring-core fiber for OAM mode transmission," Opt. Fiber Technol. **25**, 58–63 (2015).
35. L. Zhao, H. Zhao, Z. Xu, and R. Liang, "A design of novel photonic crystal fiber with low and flattened dispersion for supporting 84 orbital angular momentum modes," Commun. Theor. Phys. **73**, 085501 (2021).
36. M. Yang, W. Liu, Y. Song, J. Wang, Z. Wei, H. Meng, H. Liu, Z. Huang, L. Xiang, H. Li, and F. Wang, "A design of dual guided modes ring-based photonic crystal fiber supporting 170 + 62 OAM modes with large effective mode field area," Appl. Phys. B **128**, 38 (2022).
37. J. Tu, K. Saitoh, M. Koshiba, K. Takenaga, and S. Matsuo, "Design and analysis of large-effective-area heterogeneous trench-assisted multi-core fiber," Opt. Express **20**, 15157–15170 (2012).
38. M. F. Israk, M. A. Razzak, K. Ahmed, M. M. Hassan, M. A. Kabir, M. N. Hossain, B. K. Paul, and V. Dhasarathan, "Ring-based coil structure photonic crystal fiber for transmission of orbital angular momentum with large bandwidth: outline, investigation and analysis," Opt. Commun. **473**, 126003 (2020).
39. W. Liu, C. Liu, J. Wang, J. Lv, Y. Lv, L. Yang, N. An, Z. Yi, Q. Liu, C. Hu, and P. K. Chu, "Surface plasmon resonance sensor composed of microstructured optical fibers for monitoring of external and internal environments in biological and environmental sensing," Results Phys. **47**, 106365 (2023).
40. G. Sun, Q. Liu, H. Mu, Y. Sun, S. Wang, M. Han, J. Wang, J. Lv, P. K. Chu, and C. Liu, "Anti-resonant fiber with nested U-shape tubes for low-loss terahertz waveguides," Opt. Laser Technol. **163**, 109424 (2023).
41. T. Sun, G. Kai, Z. Wang, S. Yuan, and X. Dong, "Enhanced nonlinearity in photonic crystal fiber by germanium doping in the core region," Chin. Opt. Lett. **6**, 93–95 (2008).
42. M. M. Hassan, M. A. Kabir, M. N. Hossain, B. Biswas, B. K. Paul, and K. Ahmed, "Photonic crystal fiber for robust orbital angular momentum transmission: design and investigation," Opt. Quantum Electron. **52**, 8 (2020).
43. G. P. Agrawal, "Nonlinear fiber optics," in *Nonlinear Science at the Dawn of the 21st Century*, Vol. 542 of Lecture Notes in Physics (2001), pp. 195–211.
44. J. W. Fleming, "Dispersion in GeO_2–SiO_2 glasses," Appl. Opt. **23**, 4486–4493 (1984).